LUND UNIVERSITY

In vitro self-assembly of the light harvesting pigment-protein LH2 revealed by ultrafast spectroscopy and electron microscopy

Schubert, Axel; Stenstam, Anna; Beenken, Wichard; Herek, Jennifer; Cogdell, R; Pullerits, Tönu; Sundström, Villy

[Link to publication](#)

In Vitro Self-Assembly of the Light Harvesting Pigment-Protein LH2 Revealed by Ultrafast Spectroscopy and Electron Microscopy

Axel Schubert,* Anna Stenstam,[†] Wichard J. D. Beenken,* Jennifer L. Herek,[‡] Richard Cogdell,[§] Tõnu Pullerits,* and Villy Sundström*

*Chemical Physics, [†]Physical Chemistry 1, Lund University, Lund, Sweden; [‡]Fundamenteel Onderzoek der Materie, Institute for Atomic and Molecular Physics, Amsterdam, The Netherlands; and [§]Biochemistry and Molecular Biology, Glasgow University, Glasgow, United Kingdom

ABSTRACT   Controlled ensemble formation of protein-surfactant systems provides a fundamental concept for the realization of nanoscale devices with self-organizing capability. In this context, spectroscopic monitoring of pigment-containing proteins yields detailed structural information. Here we have studied the association behavior of the bacterial light-harvesting protein LH2 from *Rhodobacter spheroides* in an *n,n*-dimethyldodecylamine-*n*-oxide/water environment. Time-resolved studies of the excitation annihilation yielded information about aggregate sizes and packing of the protein complexes therein. The results are compared to transmission electron microscopy images of instantaneously frozen samples. Our data indicate the manifestation of different phases, which are discussed with respect to the thermodynamic equilibrium in ternary protein-surfactant-water systems. Accordingly, by varying the concentration the formation of different types of aggregates can be controlled. Conditions for the appearance of isolated LH2 complexes are defined.

INTRODUCTION

The understanding of self-organization processes in nature becomes increasingly interesting for the construction of functional units on a supramolecular level, i.e., nanodevices. Several types of organic and inorganic systems have been used recently to yield such structures with varying function-alities (Sirringhaus et al., 1999; Li et al., 1999; Ogawa et al., 2002). Charge and energy transfer processes within nanoscale arrangements of molecules have been employed for the realization of electrical gating devices with potential of forming a basis for molecular-scale information processing systems (Ambroise et al., 2001). Certain in vitro reconstituted photosynthetic proteins with genetically modified structure and pigment content can, in principle, be used for the same purpose (Wolf-Klein et al., 2002). Even native, isolated pigment proteins like bacteriorhodopsin have been investi-gated for their applicability as optical switches (Lewis et al., 1997). The formation of functional nanostructures on the basis of such nature-designed modules can benefit from their self-organization capabilities. Natural proteins organize themselves not only by forming aggregates of protein units (Rogl et al., 1998), but these aggregates also form long-range functional assemblies, such as photosynthetic systems of plants and bacteria (Sundström et al., 1999). For example, the photosynthetic systems of purple bacteria utilizing the following principle of organization have already been well established in early studies: several peripheral antenna complexes (LH2) surround the core antennae (LH1), which each enclose a reaction center. Together they form a photo-synthetic unit. The photosynthetic units are not well separated, but are instead interconnected for larger domains, where excitation transfer can take place. This organization is responsible for making the functioning of the early stages of the natural light harvesting highly efficient. Similarly, in vitro organization of biological complexes to aggregates (supra-organization) has the potential of implementing various functionalities. In this context, the self-assembly mechanisms play a key role for the viability of intelligent nanostructural arrangements. A recent work by Frese et al. (2000) has provided detailed information about long-range organization mechanisms of photosynthetic pigment-protein complexes in the photosynthetic purple bacteria. Other highly ordered arrangements of photosynthetic systems, as revealed by negative-stain-aided electron microscopy, have also been reported (Jungas et al., 1999; Bibby et al., 2001). The emerging understanding of the organization mechanisms now gradually opens the field to their application for directed ensemble formation of photoactive complexes in vitro.

The current work addresses general self-association behavior of an isolated pigment-protein complex in the presence of surfactant molecules in a polar aqueous en-vironment. We have used the peripheral light-harvesting antenna (LH2) of the purple bacterium *Rhodobacter* (*Rb.*) *spheroides*. The functional and spectroscopic properties of this extensively explored system are basically understood (Hess et al., 1995; Sundström et al., 1999). The structure of LH2 from a closely related bacterium *Rhodopseudomonas* (*Rps.*) *acidophila* has been resolved (McDermott et al., 1995). Possible minor structural differences between *Rb. spheroides* and *Rps. acidophila* do not affect the current work and hence we use the structure of the *Rps. acidophila* for analyzing our results. The protein framework of LH2 is built by nine identical subunits consisting of one α- and one β-apoprotein, thus forming a cylinder of ~6-nm in height and ~8-nm in diameter. Inside 27 bacteriochlorophyll

a (Bchl) molecules are arranged in two stacked rings. One ring, B850, is formed by 18 Bchl molecules in a water wheel-like structure; the other, B800, contains the remaining nine Bchls molecules. Due to the denser packing the B850 ring is characterized by strong electronic interaction between the Bchls, which is responsible for the bigger part of the red shift of the Q_y-absorption to 850 nm. Simultaneously, the excitation energy transfer dynamics within the ring are accelerated to a 100-fs timescale (Jimenez et al., 1996). Spectral separation of energy levels and accelerated excitation kinetics makes the B850 ring of LH2 a unique example for functional design by nature with meaningful potential for nanoengineering. Perhaps partly inspired by the LH2 complex, noticeable effort has recently been invested in the chemical synthesis of ring-like porphyrin structures for optoelectronic applications (Li et al., 1999). Compared to the synthetic structures, the protein matrix allows additional flexibility for structural and functional manipulation by mutagenesis or pigment exchange (Fowler et al., 1993; Herek et al., 2000). This enables the design of systems with distinctive excited-state dynamics, essential for optoelectronic devices (Fiedor et al., 2000). Last but not least, the native LH2 complex has a highly effective, carotenoid-driven protection system against photo damage (Young, 1991; Limantara et al., 1998).

At high light intensities it may happen that two or more excitations are simultaneously present in a given domain (i.e., an extended network of LH2 complexes). In this case excitation annihilation can take place (Mauzerall, 1976; den Hollander et al., 1983; Valkunas et al., 1995). The annihilation process is usually described as excitation transfer to an already excited molecule, where it produces a higher (doubly) excited electronic state. By very fast internal conversion the molecule relaxes to the lowest excited molecular state. The bottom line is that one excitation is lost. The same process can also be described in terms of collective excitations—i.e., excitons—by coupling the one- and two-exciton manifolds (Brüggemann et al., 2001). Previous annihilation studies, where the fluorescence quantum yield has been measured as a function of excitation pulse intensity, have provided information about the domain size of various bacterial antennas and antenna preparations (van Grondelle et al., 1983; Vos et al., 1986; Westerhuis et al., 1998). Recently, simultaneous analysis of excitation annihilation dynamics and transient absorption anisotropy decay in well-separated rings of LH2 has been used for obtaining detailed information about excited state properties and dynamics in a B850 ring (Trinkunas et al., 2001). In the current work we extend the above study from the single B850 ring to aggregates, where efficient *inter*-ring excitation transfer takes place. The aggregation behavior of LH2 is studied as a function of different protein/surfactant concentrations in excess buffer environment using *n,n*-dimethyldodecylamine-*n*-oxide (LDAO) as surfactant. Dissolving the LH2 complex in buffered LDAO-solution is chemically equivalent to a pseudoternary protein-surfactant system (Tanford, 1997). In such systems, nonpolar hydrocarbon chains of surfactant molecules can be adsorbed at hydrophobic parts of the protein surface. As such, the polar headgroups of the surfactant molecules are arranged as a hydrophilic outer surface and enable the dissolution in polar environments like water (Evans and Wennerström, 1999). Ternary protein-surfactant-water systems are known to equilibrate in different phases depending on the molar concentration ratios of the constituents. This process has been studied for a large variety of systems (Morén et al., 1999; Vasilescu et al., 1999; Jones et al., 1996). Accordingly, distinct phases correspond to different arrangements of the components, or, in other words, different species of aggregates. The overwhelming number of studies concerning the interaction between membrane proteins and surfactant molecules has been focused on either membrane solubilization or crystallization of solubilized complexes (Le Maire et al., 2000; Roth et al., 1989). Here we investigate the protein-surfactant system over an intermediate LH2/LDAO concentration range. The results of the analysis of the ultrafast spectroscopy measurements are combined with information from transmission-electron microscopy (TEM) images of instantaneously frozen samples. This approach leads to detailed information about the aggregate structure and size.

MATERIALS AND METHODS

Sample preparation

LH2 complexes were isolated from *Rb. spheroides* as previously described (Hawthornthwaite and Cogdell, 1991) and the stock solution was stored at −70°C. It contained the isolated complex LH2 in TRIS buffer at pH = 8.0 and 0.15 mM LDAO as surfactant. Note that, at this pH, LDAO is nonionic, inasmuch as the reported pK value is 5 (Maeda et al., 1974). To vary the concentrations of LH2 and LDAO, the samples were prepared by adding the appropriate amount of LDAO and buffer solution (pH 8.0) immediately after thawing the LH2 stock solution. All measurements were started after 10 min of equilibration time at a constant temperature of 20°C. Under these conditions the critical micellar concentration (CMC) of LDAO in water is 1.2 mM (Mizoguchi et al., 2002). The integrity of the LH2 complexes before and after the measurement was monitored by steady-state absorption measurements using a Jasco-V530 absorption spectrometer (JASCO, AS Maarssen, The Netherlands).

Spectroscopy

Time-dependent pump-probe spectra were recorded using 120-fs laser pulses in a spectrometer setup as described in detail previously (Polivka et al., 2000). In short, an optical parametric amplifier (TOPAS) pumped by an amplified Ti:Sapphire laser system (Spectra-Physics, Mountain View, CA) was used to yield excitation pulses at 845 nm central wavelength (spectral width: 10 nm full width at half-maximum). The pump pulse is temporarily shifted with respect to the probe pulse by an optical delay line. White-light continuum (cutoff below 800 nm) was used as probe beam and the absorption changes measured in 2-mm cuvettes were detected at 875 nm. The intensity applied for the excitation annihilation measurements was 60 μW in a spot with 350-μm diameter at 5 kHz repetition rate, corresponding to a photon density of 5×10^{13} photons cm^{-2} per pulse.

Electron microscopy

To obtain preparations for TEM imaging, a drop of the sample (~8 μl) was placed on a lacy carbon film supported by a 100-nm-thick copper grid. The formation of concave films with thicknesses of 100 nm at the edge and ~30 nm in the center was obtained by blotting in a controlled-environment vitrification system. To prevent water crystallization, the grids were frozen instantaneously by plunging into liquid ethane at its freezing point. Samples were then transferred under nitrogen atmosphere to a Phillips cryoelectron microscope (CM 120 Bio TWIN, Phillips, Eindhoven, The Netherlands) and measurements were run as described previously (Morén et al., 1999). The electron microscope was operated at an acceleration voltage of 120 kV.

RESULTS

Ultrafast spectroscopy

Fig. 1 shows transient absorption kinetics after direct excitation of the B850 band as obtained for various LDAO concentrations in the case of an LH2 solution with optical density (OD) of 0.02 at 850 nm, which corresponds to 0.06 μM LH2 complexes. (This has been calculated by using the molar extinction coefficient $\varepsilon = 90$ mM^{-1} cm^{-1} at the Q_y-band maximum of Bchl; see Hoff and Amesz, 1991. Extinction of the B850 band of LH2 is taken for 18 Bchl molecules. Finally, the area under the Q_y-absorption band of Bchl has been adapted to the ~1.5-times wider B850 band of LH2. The resulting concentration conversion factor is 3 μM LH2 per OD for the 2-mm cuvette used here.) In all curves a subpicosecond component is present reflecting the initial *intra*-ring annihilation for the B850 rings that are multiply excited by the laser pulse. The slower dynamics contain two different components: the single-excitation decay and the *inter*-ring annihilation. These dynamics depend strongly on the aggregation state of LH2. In the case of higher LDAO

concentration ($c_{LDAO} = 1.5–15$ mM), after the initial *intra*-ring annihilation only the exponential single-excitation decay occurs with a time constant of $\tau \approx 750$ ps corresponding well to the previously reported excitation lifetimes of ~1 ns (Bergström et al., 1988; Monshouwer et al., 1997). This means that conditions are achieved where the LH2 complexes are well separated (Trinkunas et al., 2001). For LDAO concentrations >15 mM, the LH2 complexes decompose, as indicated by fluorescence of free Bchl (not shown). For lower LDAO concentrations ($c_{LDAO} = 0.15$ mM and 0.5 mM), the decay of the signal is faster and nonexponential due to *inter*-ring annihilation, which indicates aggregation of the LH2 protein complexes.

Similar sets of kinetics were measured for samples of higher concentrations of LH2 ($c_{LH2} = 0.3, 1.5,$ and 6 μM; Figs. 2–4). The sensitivity of the transient absorption measurements is dramatically reduced for LH2 concentrations <15 nM (Fig. 5) and >6 μM due to the optical density being too low or too high, respectively. In total we measured transient absorption kinetics for 25 different combinations of LH2 and LDAO concentrations. Qualitatively all these kinetics show a similar behavior as those in Fig. 1. Below the CMC of LDAO (1.2 mM), and independent of the LH2 concentration, all measurements produce nonexponential decay curves for *inter*-ring annihilation indicating an aggregation of the LH2 complexes. Interestingly, above the CMC there exists a region of concentrations (see Fig. 7, *region II*) where the kinetics are relatively slow (compare Figs. 2 and 3, $\circ$, as well as Figs. 3 and 4, $\triangle$) but do not correspond to the single-excitation decay. Consequently, under these conditions aggregates of LH2 complexes are formed that are different from those obtained at LDAO concentrations below the CMC. These qualitative statements will be
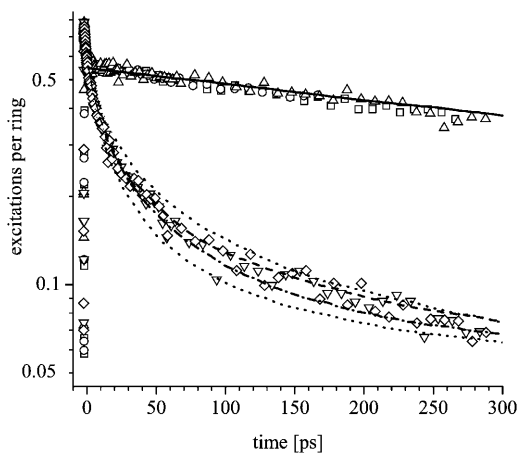
FIGURE 1   Kinetics for samples with optical density (OD) of 0.02 ($c_{LH2} = 0.06$ μM) at different surfactant concentrations: $c_{LDAO} = 15$ mM ($\square$), 5 mM ($\circ$), 1.5 mM ($\triangle$), 0.5 mM ($\triangledown$), and 0.15 mM ($\diamond$). Furthermore, simulations are shown for aggregate sizes $N = 1$ (*solid line*), 10 (*dashed line*), and 12 (*dash-dotted line*), all with a ring-to-ring hopping rate $k = 30$ ns^{-1}. For $N = 12$, simulations with $k = 20$ ns^{-1} (*upper dotted line*) and 40 ns^{-1} (*lower dotted line*) mark the confidence band.
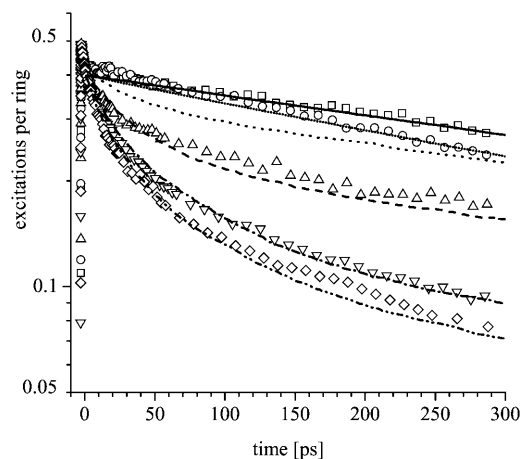
FIGURE 2   Kinetics for samples with $c_{LH2} = 6$ μM (OD = 2) and $c_{LDAO} = 15$ mM ($\square$), 5 mM ($\circ$), 1.5 mM ($\triangle$), 0.5 mM ($\triangledown$), and 0.15 mM ($\diamond$). Simulations are shown for $N = 1$ (*solid line*), 2 (*thick dotted line*), 4 (*dashed line*), 9 (*dash-dot-dotted line*), and 12 (*dash-dot-dotted line*), all with $k = 15$ ns^{-1}. The kinetics for 5 mM LDAO ($\circ$) fits best to simulation with $N \gg 10$ and $k = 0.3$ ns^{-1} (*thin dotted line*).

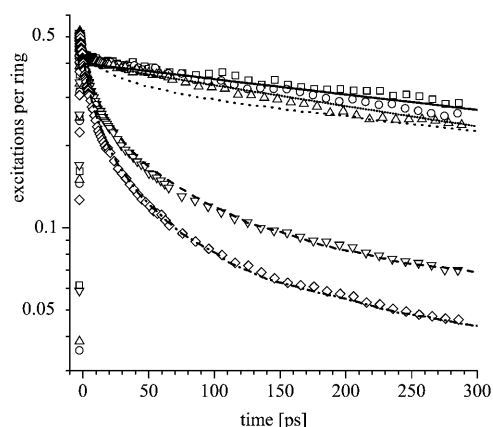FIGURE 3   Kinetics for samples with $c_{LH2} = 1.5\ \mu M$ (OD = 0.5) and $c_{LDAO} = 15$ mM ($\square$), 5 mM ($\bigcirc$), 1.5 mM ($\triangle$), 0.5 mM ($\triangledown$), and 0.15 mM ($\diamond$). Simulations are shown for $N = 1$ (*solid line*), $N = 12$ with $k = 25\ ns^{-1}$ (*dashed line*), and $N = 18$ with $k = 40\ ns^{-1}$ (*dash-dotted line*). Here the kinetics for 1.5 mM LDAO ($\triangle$) fits much better to the simulation with $N \gg 10$ but $k = 0.3\ ns^{-1}$ (*thin dotted line*) than to one with $N = 2$ with $k = 15\ ns^{-1}$ (*thick dotted line*).

confirmed by quantitative analysis, which compares the measured kinetics with simulations of the *inter*-ring annihilation dynamics in LH2 aggregates.

Electron microscopy

The results obtained by ultrafast spectroscopy are complemented by TEM studies of instantaneously frozen samples with 2–3-nm resolution at different protein/surfactant concentrations as shown in Fig. 6 (for concentrations, see figure legend). Although the resolution of such samples is lower than the negative-stained preparations on surfaces, the freeze
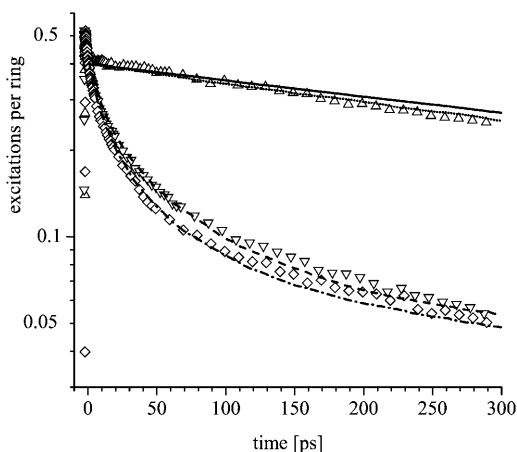

FIGURE 4   Kinetics for samples with $c_{LH2} = 0.3\ \mu M$ (OD = 0.1) and $c_{LDAO} = 1.5$ mM ($\triangle$), 0.5 mM ($\triangledown$), and 0.15 mM ($\diamond$). Simulations are shown for $N = 1$ (*solid line*), $N = 16$ with either $k = 30\ ns^{-1}$ (*dashed line*), or $k = 40\ ns^{-1}$ (*dash-dotted line*). For 1.5 mM LDAO ($\triangle$), the kinetic track fits best to simulation with $N \gg 10$ and $k = 0.1\ ns^{-1}$ (*dotted line*). Kinetics for $c_{LDAO} = 15$ mM and 5 mM are not shown here for different number of initial excitations, but both fit to simulation with $N = 1$.
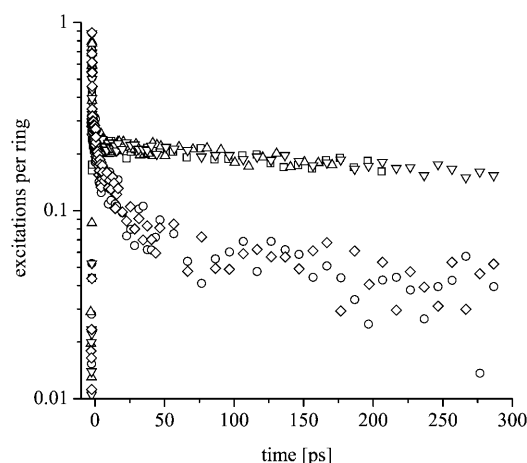

FIGURE 5   Kinetics for samples with $c_{LH2} = 15$ nM (OD = 0.005) and $c_{LDAO} = 15$ mM ($\square$), 5 mM ($\bigcirc$), 1.5 mM ($\triangle$), 0.5 mM ($\triangledown$), and 0.15 mM ($\diamond$). No simulations.

process guarantees a much better preservation of the initial aggregation state during sample fixation.

Fig. 6 *A* presents a typical image of LH2 complexes at nonaggregated conditions ($c_{LH2} = 6\ \mu M$ and $c_{LDAO} = 15$ mM). In contrast to the pure LDAO/buffer solution (Fig. 6 *B*), dark spots can clearly be seen in the image. The diameter of the spots is ~ 10 nm and there is, on average, one spot per area of 50 nm $\times$ 50 nm. The thickness of the sample is 50–100 nm leading to an estimate of 10 μM LH2. The size and concentration match very well what would be expected for the well-separated LH2 complexes and support the conclusions drawn from ultrafast spectroscopy (compare to Fig. 2, $\square$). For LDAO concentrations below the CMC, small cluster-like aggregates with varying shape and sizes of up to 35 nm are obtained (Fig. 6 *E*), but also very few rather huge assemblies (Fig. 6 *F*). In the special region of LH2 and LDAO concentrations where annihilation is slow (see above), the formation of sheet-like aggregates is observed. For example, at $c_{LH2} = 1.5\ \mu M$ and $c_{LDAO} = 5$ mM, one can see several structured areas (Fig. 6 *C*). Fourier transformation of the marked square (Fig. 6 *D*) reveals that in this area the LH2 aggregates form a hexagonal lattice in a two-dimensional layer. The formation of two-dimensional layers is indicated by the edge (Fig. 6 *C*, *lower area*) producing a line of intense contrast. These extended, sheet-like aggregates are different from the smaller, cluster-like ones obtained at LDAO concentrations below the CMC. To quantify these results in terms of different packing densities of the aggregates, the TEM resolution has not been sufficient. In particular for the tiny aggregates shown in Fig. 6 *E*, Fourier analysis is not possible.

Simulations

To establish the initial conditions of the simulations, we first analyzed the fast *intra*-ring annihilation at the beginning of
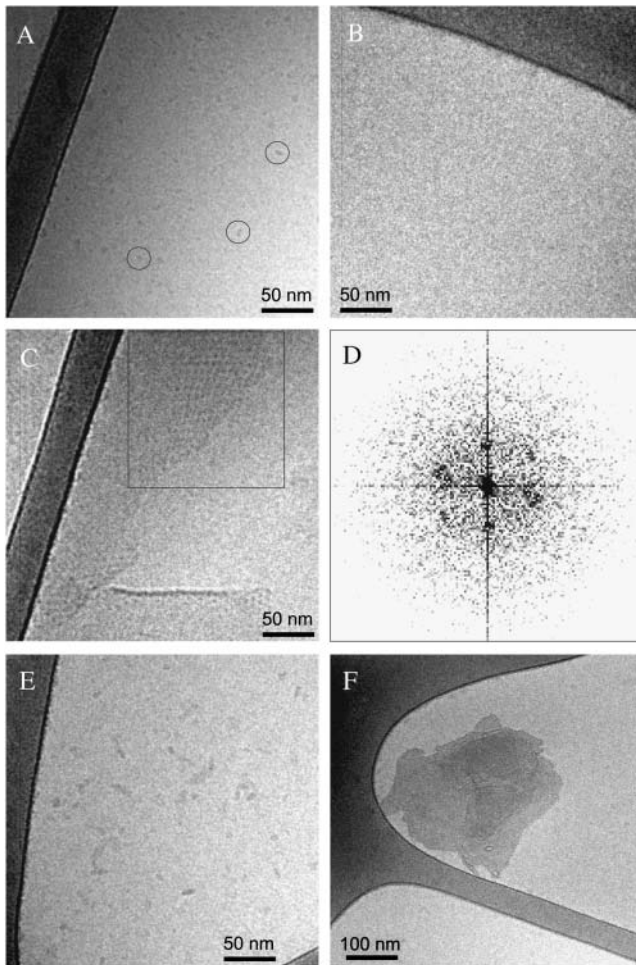
FIGURE 6 TEM images for different LH2 and LDAO concentrations. (A) $c_{LH2} = 6\ \mu M$, $c_{LDAO} = 15$ mM (three of several specks representing single LH2 complexes are emphasized by circles); (B) no LH2, $c_{LDAO} = 5$ mM; (C) $c_{LH2} = 1.5\ \mu M$ and $c_{LDAO} = 1.5$ mM; (D) Fourier transformation of the marked area in C; and (E and F) $c_{LH2} = 6\ \mu M$ and $c_{LDAO} = 0.15$ mM.

$$\frac{p_{\geq 1}}{18f} = \frac{1 - (1-f)^{18}}{18f} = (80 \pm 5)\%, \tag{1}$$

which results in $f = (2.7 \pm 0.8)\%$ and subsequently in $p_{\geq 1} = (40 \pm 10)\%$. The latter is the initial occupation for the simulations of *inter*-ring annihilation after completion of the initial *intra*-ring annihilation. We have also estimated f using the absorption cross section of the Bchl, the energy of the laser pulse, and the diameter of the beam. The results are similar but the error of such an estimation is significantly larger. Hence, in what follows we will only use values of the initial population as obtained from the *intra*-ring annihilation analysis for each set of curves separately (see Figs. 1–5).

The population kinetics of the *inter*-ring annihilation process are modeled by random walks of the hopping excitations on a two-dimensional hexagonal lattice of N nodes, each representing one B850-ring. The hexagonal coordination of the lattice is strongly suggested by the TEM images (see Fig. 6, C and D). It is also the most favorable structure with respect to the surface polarity distribution. For the same reason the N nodes are arranged for a minimum perimeter of the aggregate. At the beginning of each simulation track, some of the N lattice-nodes are randomly occupied by single excitations with probability $p_{\geq 1}$ as obtained from the previous analysis of the *intra*-ring annihilation. Thus the initial state of the simulation describes the situation immediately after the fast *intra*-ring annihilation has been completed. The subsequent random-walk simulation by means of the Monte Carlo method has been performed in short time-steps Δt (here 0.1 ps) as follows:

1. During a time-step each excitation has a probability $\Delta t/\tau$ to decay due to the single-excitation decay $\tau = 750$ ps. The decision to remove the excitation is taken from a uniform random distribution via the Monte Carlo method.

2. For the excitations that remain after step 1 we need to decide whether they make a jump or stay where they are during the time-step. The probability to jump is given as $P = N k \Delta t$, where n is the number of nearest neighbors ($N = 6$ for the rings inside the aggregate but $N < 6$ for the rings on the edges) and k is the ring-to-ring hopping rate for the *inter*-ring excitation transfer. The decision to jump is taken using the same Monte Carlo method as in step 1.

3. If the excitation is to jump, the acceptor node is chosen from a uniform distribution of the n nearest-neighbors. This condition means that k does not depend on the acceptor state but is the same for the acceptors with and without excitation. This assumption is justified by the fact that the B850 ring contains 18 Bchl molecules and even if the excitation is delocalized over 2–4 Bchl molecules (Pullerits et al., 1996; Trinkunas et al., 2001) the accepting Bchls remain most of the time unaffected.

4. If the jump is made the source node occupation is set to *0* and that of the target node is set to *1*, independent of

each kinetic trace. This enabled us to determine the fraction of initially excited B850-rings (Trinkunas et al., 2001). The initial signal intensity before *intra*-ring annihilation is proportional to the fraction f of excited Bchl molecules. According to the binominal distribution, for 18 Bchls per B850-ring the fraction of rings which contains *no* excitation is $p_0 = (1-f)^{18}$. Consequently, the fraction of rings which carry initially one or more excitations is given by $p_{\geq 1} = 1 - p_0$. After completion of the initial *intra*-ring annihilation, all these rings carry only one excitation. Correspondingly the fraction of excited Bchls is now $p_{\geq 1}/18$. The signal intensity after *intra*-ring annihilation is proportional to that number. Comparing the amplitude of the transient absorption signal after completion of the *intra*-ring annihilation with the initial amplitude we can obtain $p_{\geq 1}/(18\ f)$ directly from the experimental curves. For example, from the uppermost curve in Fig. 2 ($\square$), we estimate that the remaining signal after the *intra*-ring annihilation is ~80%, giving

whether or not the latter is already occupied. This means that if the acceptor already had an excitation, one of the two initial excitations is annihilated.

5. The procedure is carried out for all remaining excitations.
6. The time t is increased by one time-step Δt and the algorithm is repeated until $t = 300$ ps.
7. At $t = 300$ ps, a new track is started for a new random initial occupation of the same lattice.

For good statistics, 1000 simulations are accumulated for each combination of fitting parameters k and N. In the case of no aggregation—i.e., $N = 1$—the only kinetic component after *intra*-ring annihilation has occurred (see Fig. 1, *solid lines*) is the single-exponential quenching with $\tau = 750$ ps. In LH2 aggregates where the ring-to-ring hopping rate k is much higher than the single-excitation decay rate τ^{-1}, the calculated kinetics depend on the two fitting parameters in qualitatively different ways. The parameter k mainly determines the initial time-profile of the annihilation part of the decay, e.g., for $k = 20$ and 40 ns^{-1} in Fig. 1 (*dotted lines*), whereas the relative amplitude of the asymptotic exponential decay at long times determines the aggregate size N, e.g., for $N = 10$ and 12 in Fig. 1 (*dashed lines*). The latter can be understood as follows. From the $p_{\geq 1} \times N$ nodes, which are excited immediately after *intra*-ring annihilation, only one carries an excitation after *inter*-ring annihilation. Hence, the signal amplitude after completing the *intra*-ring annihilation is $p_{\geq 1} \times N$ times larger than the signal corresponding to the last excitation when interpolated to $t = 0$ for the single excitation decay. Thus, the parameters k and N are independently determinable.

If the ring-to-ring distance is so large that the excitation hopping transfer is much slower than the single-excitation decay, the aggregate size N cannot be determined from the kinetics. Nevertheless, this case can be distinguished from the nonaggregated case $N = 1$ as well as from small aggregates (e.g., $N = 2$) with ring-to-ring hopping rates $k \geq \tau^{-1}$ (compare *solid*, *thick*, and *thin dotted lines* in Fig. 2). Hence, ring-to-ring hopping rates k much lower than the single-excitation decay rate can be determined, and for $N > 10$, as suggested by the TEM image (Fig. 6 C), the k-values are independent of the aggregate size.

So far we have assumed that all the LH2 complexes are oriented in the same way in the aggregate. The fact that for two purple bacteria good quality crystals of LH2 have been made supports such an assumption. However, LH2 of *Rb. spheroides* has not yet been crystallized. Furthermore, the LDAO present in vitro may form a layer around the waists of the cylindrical LH2 complexes (Prince et al., 2003). Consequently, we need to consider the possibility that within an aggregate some LH2 complexes may be oriented upside-down. We have simulated random walks on a hexagonal lattice where two types of nodes are randomly distributed, representing the two orientations of LH2 complexes. Between oppositely oriented rings we use the ring-to-ring

hopping rate k' instead of k, which is used between LH2 complexes with the same orientation. Because the B850 ring, which carries the excitation, is not located in the center of the LH2 cylinder, the effective distance for the hopping transfer is increased for the differently oriented LH2 complexes. We have estimated (by using Eq. 2) that this will slow down the transfer rate for oppositely oriented LH2 by a factor of 5—i.e., $k'/k \approx 20\%$. To resemble the same kinetics, the model of arbitrarily oriented LH2 complexes needs almost two-times higher hopping rates k compared to the values used for aggregates with uniformly oriented LH2 complexes. The aggregate size parameter N, however, is nearly independent of the choice of the model. In what follows, a uniform orientation of the LH2 complexes in respect of the two-dimensional aggregates is assumed. The results, however, can be easily transferred to the case of arbitrarily oriented LH2 complexes (i.e., 50% upside-down) by rescaling the value of the ring-to-ring hopping rates k by a factor of 2. A similar rescaling, but in the opposite direction, would be necessary for double layers of stacked LH2 complexes with the B850 rings facing each other (compare to Prince et al., 2003). Note that, in the present context, N has the meaning of the number of effectively coupled rings, rather than that of the full three-dimensional size of a loosely packed aggregate.

By varying the parameters N and k we have fitted our simulations to the measured kinetics (Figs. 1–5). In Fig. 7 the results of these fits for all measured combinations of LH2 and LDAO concentrations are summarized. Three different regions are found:

1. For LDAO concentrations below the CMC ($c_{LDAO} < 1.2$ mM), the aggregate size is $N = 14 \pm 4$ and ring-to-ring hopping rate is $k = 30 \pm 15$ ns^{-1} (Figs. 1–5, *dashed* and *dash-dotted lines*). These aggregate sizes fit remarkably well to the sizes of the spots observed in the TEM images
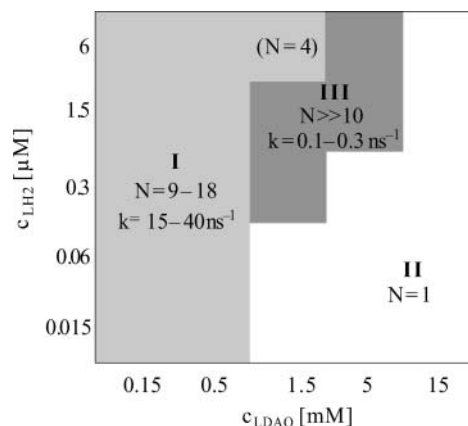

FIGURE 7 Plot presenting the relevant aggregation parameters N and k in dependence of the LH2 and LDAO concentrations, as obtained from simulations of the kinetics shown in Figs. 1–5. Three regions (*I–III*), where different types of LH2 aggregates occur, are marked by shading (see text).

(Fig. 6 E). For $c_{LH2} = 6\ \mu M$ and $c_{LDAO} = 1.5\ mM$, which is above the CMC, one obtains similar ring-to-ring hopping rates but with much smaller aggregate sizes ($N = 4$).

2. Isolated LH2 complexes are indicated by the fitting parameters $N = 1$ and $k = 0$. For LH2 concentrations $<0.3\ \mu M$ these conditions are obtained for LDAO concentration just above the CMC. For increased LH2 concentrations higher LDAO concentrations are needed to solubilize the LH2 complexes completely. Note that LDAO concentrations >15 mM disintegrates the LH2 complexes.

3. For concentrations between the regions I and II, the best fit is obtained for ring-to-ring hopping rates k between 0.1 and 0.9 ns^{-1}, which are significantly lower than the single-excitation decay rate τ^{-1} of 1.3 ns^{-1}. As mentioned above, in these cases a determination of the aggregate size from the ultrafast spectroscopy is not possible. However, the TEM images for corresponding concentrations show extended layers of hexagonally arranged aggregates (Fig. 6 C). Hence, we assumed aggregate sizes of $N \gg 10$, and determined k more precisely to values of $0.3 \pm 0.1\ ns^{-1}$ (Figs. 2 and 3, *thin dotted lines*) for the combinations of concentration $c_{LH2}/c_{LDAO} = 6\ \mu M/5\ mM$ and 1.5 $\mu M/1.5$ mM (Fig. 2, ○, and Fig. 3, △, respectively). By comparison of the data with the simulations for $N = 2$ (Figs. 2 and 3, *thick dotted lines*), it can be clearly excluded that the respective kinetics result from small aggregates with similar ring-to-ring hopping rates k as found for LDAO concentrations below the CMC (region I). The kinetics for the concentration combinations 0.3 $\mu M/1.5$ mM and 0.3 $\mu M/1.5$ mM (Fig. 3, ○, and Fig. 4, △, respectively) fit best to extended aggregates with hopping rates $k = 0.1 \pm 0.1\ ns^{-1}$ (compare to Fig. 4), but can be also interpreted as a result of isolated LH2 ($N = 1$, Figs. 3 and 4, *solid lines*).

DISCUSSION

The most common method to determine the size of aggregates is perhaps dynamic light scattering (Brown, 1993). In the presented work we have demonstrated how self-assembly processes in a protein-surfactant system can be monitored by excitation annihilation using ultrafast spectroscopy. The very different values of the ring-to-ring hopping rate for different compositions (Fig. 7) have clearly indicated the formation of two well-distinguishable types of aggregates in the LH2-LDAO-water system. Before this will be discussed in the framework of a typical phase diagram for ternary protein-surfactant-water systems, we further explain the relevance of the parameter k for the packing of the LH2 complexes in the different types of aggregates. Note that this kind of information cannot be obtained by dynamic light scattering.

Hopping rate and ring-to-ring distance

In principle, the value of k can be related to the ring-to-ring distance of Förster's equation (Förster, 1948), based on the dipole-dipole interaction given for the hopping rate,

$$k = \frac{1}{\tau_{fl}} \left(\frac{R_0}{R} \right)^6, \tag{2}$$

where τ_{fl} is the radiative lifetime of the B850 excitation (not to be mixed up with the single-excitation lifetime τ mentioned above) and R_0 is the so-called Förster radius which contains the spectral overlap between donor and acceptor of the excitation. In the present case, however, the relation between hopping rate k and ring-to-ring distance R is not so simple. The reason lies in the properties of B850 excited state and the *intra*-ring excitation dynamics. Detailed studies of the *intra*-ring annihilation have revealed that the excitation is delocalized over 2–4 Bchls of the B850-ring (Trinkunas et al., 2001), forming a molecular exciton. Numerous other studies have yielded similar results (Pullerits et al., 1996; Chachisvilis et al., 1997; Monshouwer et al., 1997; Dahlbom et al., 2001). As mentioned above, the exciton dynamics inside the B850 ring are much faster than the *inter*-ring dynamics. Hence, to determine the ring-to-ring hopping rate one must evaluate the hopping rates for all possible positions of the exciton and average over them. In this procedure the use of Eq. 2 may involve very large errors. In fact for an extended excitation the point-dipole approximation may fail (Scholes, 1999) and Eq. 2 is not applicable. Consequently we will use it only for qualitative discussions. A more rigorous calculation of the distance R from the ring-to-ring hopping rate k goes beyond the scope of the current study and will be the subject for future work.

The ring-to-ring hopping rate $k = 30 \pm 15\ ns^{-1}$ (corresponding time is $\sim$30 ps) found for the cluster-like aggregates at LDAO concentrations below the CMC (Fig. 7, *region I*) means that for a B850-ring surrounded by six neighboring rings the excitation residence time is $\sim$5 ps. This number is remarkably close to the low-temperature dephasing time of 6.6 ps measured by spectral hole-burning at the red edge of the B850-band in native LH2 membranes (Reddy et al., 1992). On the other hand, measurements of the excitation transfer from the peripheral antenna LH2 to the core antenna LH1 in native membranes have given a range of transfer times, e.g., 3.3 ps (Hess et al., 1995), 4.5 ps (Nagarajan and Parson, 1997), and 8 ps (Freiberg et al., 1989). Notably, Nagarajan and Parson as well as Freiberg and co-workers also found a slower transfer component of $\sim$25 ps. Nevertheless, our results cannot exclude that in the small, cluster-like LH2 aggregates formed below the CMC of LDAO (compare to Fig. 6 E), the LH2 complexes are still separated by a thin layer of surfactant molecules or residual membrane lipids. However, for the sheet-like type of aggregates (compare to Fig. 6 C) formed at LH2/LDAO

concentrations in region II above the CMC, the ring-to-ring distances are significantly larger. From Eq. 2 one can estimate that the distance R relevant for the Förster transfer is approximately twice as large as in the first type of aggregates. Note that R does not mean the ring-to-ring distance but the distance from the effective donor to the effective acceptor situated on the neighboring rings. The additional space between the hydrophobic waists of the cylindrical LH2 complexes is apparently filled by surfactant molecules, which in this case do not solubilize the LH2 complexes completely, but rather organize them in a two-dimensional hexagonal lattice as shown in Fig. 6 C.

Ternary LH2-LDAO-water system

The combination of ultrafast spectroscopy results (fitted by random-walk simulations) and cryo-TEM have identified three different types of aggregates. In the preceding text they were characterized as isolated LH2 complexes ($N = 1$), cluster-like aggregates of nonsolubilized LH2 ($N \approx 14$) and sheet-like aggregates ($N \gg 10$). The occurrence of these structures depends on the concentrations of LH2 and LDAO as has been illustrated in Fig. 7. However, to understand the specific aggregation behavior a thermodynamic phase diagram should be considered—as presented in Fig. 8. This phase diagram is a generalized qualitative description of the behavior of the ternary protein-surfactant-water system. The basis is given by the binary LDAO-water system, with the micellar L_1 and the lamellar liquid crystalline phase L_α (Lutton, 1966). When a third amphiphilic component like the LH2 complex with hydrophobic and hydrophilic regions is subjected to this binary system, the balance between hydrophobic and electrostatic interactions that dominate the structural behavior is strongly affected (Jönsson and Wennerström, 1987; Landgren et al., 1992). Jönsson and Wennerström (1987) developed a thermodynamical model for this mechanism, which predicts that the lamellar phase L_α swells to dilute conditions for increased LH2 concentrations. The qualitative phase diagram (Fig. 8) is based on this approach. A similar phase diagram has been presented for another membrane-spanning protein, gramicidin, in aqueous LDAO (Orädd et al., 1995).

Due to the swelling of the lamellar phase L_α even at the low concentration of LDAO used in our samples, we have to consider three phases, which are related to the three different aggregation states of the LH2 complexes. Isolated LH2 complexes ($N = 1$) occur in the micellar phase L_1 above the CMC. Note that in the premicellar L_1-phase, i.e., below the CMC of LDAO, the LH2 complexes do not solubilize as well as in the micellar L_1-phase (compare to Jönsson and Wennerström, 1987). Therefore at LDAO concentrations lower than the CMC the LH2 complexes form small but densely aggregated clusters with size $N = 14 \pm 4$, as detected by ultrafast spectroscopy as well as the TEM images (Fig. 6 E). In the phase diagram these are represented by the top corner. The extended hexagonal but less densely packed aggregates ($N \gg 10$) are assigned to the liquid crystalline lamellar phase L_α. The edge that appears in the TEM image (Fig. 6 C) clearly shows the lamellar sheet-like structure of these aggregates. Similar self-assembly has been shown for several membrane proteins since the pioneering study of the bacteriorhodopsin-surfactant-water system by Unwin and co-worker (Henderson and Unwin, 1975; Unwin and Henderson, 1975).

For the quite-low concentrations of LH2 but also of LDAO, our samples are located in the water-rich corner of the phase diagram (Fig. 8 b). At the lowest concentrations of LDAO used in the present work ($c_{LDAO} < 1.5$ mM), the LH2-poor premicellar L_1-phase—i.e., the region between the critical association concentration and the CMC—coexists with undissolved LH2 as represented by the cluster-like aggregates. Increasing LDAO concentration leads to two possible phase transitions: For low LH2 concentration one will pass the CMC and reach directly the micellar region of the L_1-phase, where the whole LH2 content is completely solubilized ($N = 1$). For higher LH2 concentrations ($c_{LH2} = 0.5$–5 μM), however, one will reach a region in the phase diagram where the L_1-phase coexists with the lamellar L_α-phase. The ultrafast spectroscopy results suggest that in this case the majority of the LH2 content is incorporated into
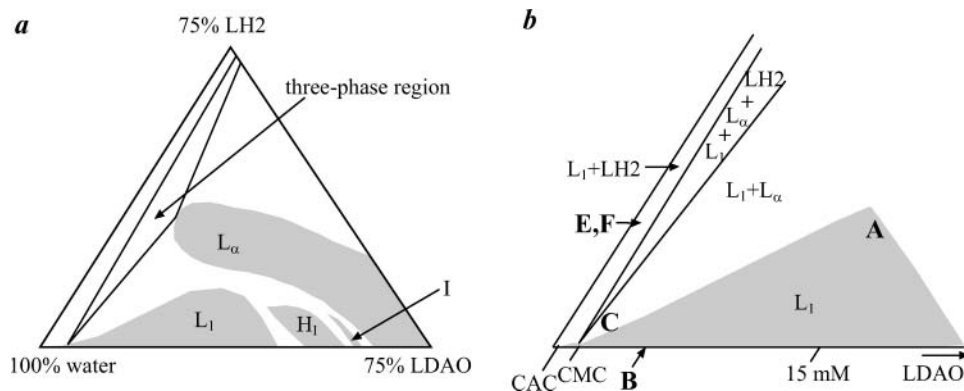
FIGURE 8 Qualitative phase diagram of the ternary system LH2-LDAO-water. (a) LH2, densely aggregated protein complexes; L_1, micellar phase; L_α, lamellar phase; H_I, hexagonal phase; and I, cubic phase. Water-rich corner of the phase diagram. (b) The L_1 phase and three regions of coexistence are assigned. The critical association concentration (CAC) as well as the critical micellar concentration (CMC) are given on the LDAO coordinate. Furthermore, the estimated positions for the TEM images are marked A–C and E and F, as in Fig. 6.

the lamellar L_α-phase. Otherwise the lamellar aggregates would not have been detected, because the contribution of the *inter*-ring annihilation to the overall signal decay would have been smaller than the signal/noise of the experiment. A similar accumulation in the lamellar L_α-phase has been reported for gramicidin (Orädd et al., 1995). In the lamellar L_α-phase the cylindrical LH2 complexes are embedded in a double layer of surfactant molecules with their hydrophobic waists surrounded by the nonpolar tails of the surfactant molecules, while the polar caps protrude the polar surfaces of the lamella (Prince et al., 2003).

The relatively well-ordered arrangement of the LH2 complexes in the lamellar L_α-phase may result from a mismatch between the thickness of the hydrophobic regions of the LH2 complexes and the LDAO bilayer (Orädd et al., 1995; Fattal and Ben-Shaul, 1993). However, in the present case the mismatch is not very big. We estimate that the vertical extension of the hydrophobic waist of the LH2 complex is ~3.5 nm (compare to Prince et al., 2003), whereas the LDAO bilayer has a thickness of ~3 nm (Evans and Wennerström, 1999). This small hydrophobic mismatch may contribute to the effective interaction between LH2 complexes, which forces them into the observed hexagonal lattice. (Note that for a given amount of surfactant to fill the interstitial areas, the hexagonal lattice results in maximum distances between the LH2 complexes, compared to other lattices, such as quadratic.) As a further consequence of this interaction the packing density of the LH2 depends on the ratio between LDAO and LH2 in the lamellar phase. An indication of such an effect is the decrease of the ring-to-ring hopping rate k from 0.3 ns^{-1} down to 0.1 ns^{-1}, if the LDAO concentration is increased, strongly suggesting that the distance between the LH2 complexes expands (compare to Fig. 3, $\bigcirc$, and Fig. 4, $\triangle$). Naturally if the ring-to-ring distance becomes too large (corresponding $k < 0.1$ ns^{-1}), one can no longer distinguish between aggregated and isolated LH2 complexes. The situation is further complicated by the fact that for increasing LDAO concentration the coexistence equilibrium between the lamellar L_α-phase and the micellar L_1-phase is shifted to the latter, where the LH2-complexes are isolated. Hence, for approaching the L_1-phase, the averaged kinetics obtain more and more the character of the single-excitation decay ($N = 1$)—i.e., the curves flatten, as for decreasing k-values.

CONCLUSIONS

In this study of the ternary system LH-LDAO-water, three types of LH2-aggregates could be identified and characterized by using a combination of ultrafast spectroscopy and cryo-TEM. In addition to small cluster-like aggregates of densely packed nonsolubilized LH2 obtained for LDAO concentrations below the CMC and isolated LH2 complexes completely solubilized in the micellar phase of LDAO, for higher LH2 concentrations and LDAO concentrations just above the CMC we have observed large hexagonal arrays of LH2 complexes. From the relatively slow excitation energy transfer on the hexagonal lattice we conclude that the LH2 complexes are not in direct contact but separated by a laminar spacer of LDAO molecules. The possible control of LH2 aggregation by the surfactant and the LH2 concentration may open a wide field of applications, but also calls for careful sample preparation in experiments intended to be conducted for single LH2 complexes.

REFERENCES

Ambroise, A., R. W. Wagner, P. D. Rao, J. A. Riggs, P. Hascoat, J. R. Diers, J. Seth, R. K. Lammi, D. F. Bocian, D. Holten, and J. S. Lindsey. 2001. Design and synthesis of porphyrin-based optoelectronic gates. *Chem. Mat.* 13:1023–1034.

Bergström, H., V. Sundström, R. van Grondelle, T. Gillbro, and R. Cogdell. 1988. Energy transfer dynamics of isolated B800–850 and B800–820 pigment-protein complexes of *Rhodobacter sphaeroides* and *Rhodopseudomonas acidophila*. *Biochim. Biophys. Acta*. 936:90–98.

Bibby, T. S., J. Nield, and J. Barber. 2001. Iron deficiency induces the formation of an antenna ring around trimeric photosystem I in cyanobacteria. *Nature*. 412:743–745.

Brown, W. 1993. Dynamic Light Scattering: The Method and Some Applications. Oxford University Press, Oxford, UK.

Brüggemann, B., J. L. Herek, V. Sundström, T. Pullerits, and V. May. 2001. Microscopic theory of excitation annihilation: application to the LH2 antenna system. *J. Phys. Chem. B*. 105:11391–11394.

Chachisvilis, M., O. Kühn, T. Pullerits, and V. Sundström. 1997. Excitons in photosynthetic purple bacteria: wavelike motion or incoherent hopping? *J. Phys. Chem. B*. 101:7275–7283.

Dahlbom, M., T. Pullerits, S. Mukamel, and V. Sundström. 2001. Exciton delocalization in the B850 light-harvesting complex: comparison of different measures. *J. Phys. Chem. B*. 105:5515–5524.

Den Hollander, W. T. F., J. G. C. Bakker, and R. Van Grondelle. 1983. Trapping loss and annihilation of excitation in a photosynthetic system I. Theoretical aspects. *Biochim. Biophys. Acta*. 725:492–507.

Evans, D. F., and H. Wennerström. 1999. The Colloidal Domain: Where Physics, Chemistry, Biology and Technology Meet. Wiley, New York, NY.

Fattal, D. R., and A. Ben-Shaul. 1993. A molecular model for lipid-protein interaction in membranes: the role of hydrophobic mismatch. *Biophys. J.* 65:1795–1809.

Fiedor, L., H. Scheer, C. N. Hunter, F. Tschirschwitz, B. Voigt, J. Ehlert, E. Nibbering, D. Leupold, and T. Elsaesser. 2000. Introduction of a 60-fs deactivation channel in the photosynthetic antenna LH1 by Ni-bacteriopheophytin a. *Chem. Phys. Lett.* 319:145–152.

Förster, T. 1948. Zwischenmolekulare energiewanderung und fluoreszenz. *Ann. Phys.* 2:55–67.

Fowler, G. J. S., W. Crielaard, R. W. Visschers, and R. van Grondelle. 1993. Site-directed mutagenesis of the LH2 light-harvesting complex of *Rhodobacter sphaeroides*: changing bLys23 to Gln results in a shift in the 850-nm absorption peak. *Photochem. Photobiol.* 57:2–5.

Freiberg, A., V. I. Godik, T. Pullerits, and K. Timpmann. 1989. Picosecond dynamics of directed excitation transfer in spectrally heterogeneous light-harvesting antenna of purple bacteria. *Biochim. Biophys. Acta.* 973: 93–104.

Frese, R. N., J. D. Olsen, R. Branvall, W. H. J. Westerhuis, C. N. Hunter, and R. van Grondelle. 2000. The long-range supraorganization of the bacterial photosynthetic unit: a key role for PufX. *Proc. Natl. Acad. Sci. USA.* 97:5197–5202.

Hawthornthwaite, A. M., and R. Cogdell. 1991. Bacteriochlorophyll binding proteins. *In* The Chlorophylls. H. Scheer, editor. CRC Press, Boca Raton, FL. 493–528.

Henderson, R., and P. N. T. Unwin. 1975. Three-dimensional model of purple membrane obtained by electron-microscopy. *Nature.* 257:28–32.

Herek, J. L., N. J. Fraser, T. Pullerits, P. Martinsson, T. Polivka, H. Scheer, R. J. Cogdell, and V. Sundström. 2000. B800–B850 energy transfer mechanism in bacterial LH2 complexes investigated by B800 pigment exchange. *Biophys. J.* 78:2590–2596.

Hess, S., M. Chachisvilis, K. Timpmann, M. R. Jones, G. J. S. Fowler, C. N. Hunter, and V. Sundström. 1995. Temporally and spectrally resolved subpicosecond energy transfer within the peripheral antenna complex (LH2) and from LH2 to the core antenna complex in photosynthetic purple bacteria. *Proc. Natl. Acad. Sci. USA.* 92:12333–12337.

Hoff, A., and J. Amesz. 1991. Visible absorption spectroscopy of chlorophylls. *In* The Chlorophylls. H. Scheer, editor. CRC Press, Boca Raton, FL. 723–738.

Jimenez, R., S. N. Dikshit, S. E. Bradforth, and G. R. Fleming. 1996. Electronic excitation transfer in the LH2 complex of *Rhodobacter sphaeroides*. *J. Phys. Chem.* 100:6825–6834.

Jönsson, B., and H. Wennerström. 1987. Phase equilibria in a three-component water-soap-alcohol system. *J. Phys. Chem.* 91:338–352.

Jones, L. S., N. B. Bam, and T. W. Randolph. 1996. Surfactant-stabilized protein formulations: a review of protein-surfactant interactions and novel analytical methodologies. *ACS Sym. Ser.* 675:206–222.

Jungas, C., J.-L. Ranck, J.-L. Rigaud, P. Joliot, and A. Verméglio. 1999. Supramolecular organization of the photosynthetic apparatus of *Rhodobacter sphaeroides*. *EMBO J.* 18:534–542.

Landgren, M., M. Aamodt, and B. Jönsson. 1992. Solubilization of uncharged molecules in ionic surfactant aggregates. 2. Phase equilibria. *J. Phys. Chem.* 96:950–961.

Lewis, A., Y. Albeck, Z. Lange, J. Benchowski, and G. Weizman. 1997. Optical communication with negative light intensity with a plastic bacteriorhodopsin film. *Science.* 275:1462–1464.

Le Maire, M., P. Champeil, and J. V. Moller. 2000. Interaction of membrane proteins and lipids with solubilizing detergents. *Biochim. Biophys. Acta.* 1508:86–111.

Li, J., A. Ambroise, S. I. Yang, J. R. Diers, J. Seth, C. R. Wack, D. F. Bocian, D. Holten, and J. S. Lindsey. 1999. Template-directed synthesis, excited-state photodynamics, and electronic communication in a hexameric wheel of porphyrins. *J. Am. Chem. Soc.* 121:8927–8940.

Li, M., H. Schnablegger, and S. Mann. 1999. Coupled synthesis and self-assembly of nanoparticles to give structures with controlled organization. *Nature.* 402:393–395.

Limantara, L., R. Fujii, J.-P. Zhang, T. Kakuno, H. Hara, A. Kawamori, T. Yagura, R. J. Cogdell, and Y. Koyama. 1998. Generation of triplet and cation radical bacteriochlorophyll a in carotenoidless LH1 and LH2 antenna complexes from *Rhodobacter sphaeroides*. *Biochemistry.* 37:17469–17486.

Lutton, E. S. 1966. Phase behavior of the dimethyldodecylamine oxide-H_2O system. *J. Am. Oil Chem. Soc.* 43:28–30.

Maeda, H., M. A. Tsunoda, and S. Ikeda. 1974. Electric and nonelectric interactions of a nonionic-cationic micelle. *J. Phys. Chem.* 78:1086–1090.

Mauzerall, D. 1976. Multiple excitations in photosynthetic systems. *Biophys. J.* 16:87–91.

McDermott, G., S. M. Prince, A. A. Freer, A. M. Hawthornthwaite-Lawless, M. Z. Papiz, R. J. Cogdell, and N. W. Isaacs. 1995. Crystal

structure of an integral membrane light-harvesting complex from photosynthetic bacteria. *Nature.* 374:517–521.

Mizoguchi, K., K. Fukui, H. Yanagishita, T. Nakane, and T. Nakata. 2002. Ultrafiltration behavior of a new type of non-ionic surfactant around the CMC. *J. Membr. Sci.* 208:285–288.

Monshouwer, R., M. Abrahamsson, F. van Mourik, and R. van Grondelle. 1997. Superradiance and exciton delocalization in bacterial photosynthetic light-harvesting systems. *J. Phys. Chem. B.* 101:7241–7248.

Morén, A. K., O. Regev, and A. Khan. 1999. A cryo-TEM study of protein-surfactant gels and solutions. *J. Colloid. Interf. Sci.* 222:170–178.

Nagarajan, V., and W. W. Parson. 1997. Excitation energy transfer between the B850 and B875 antenna complexes of *Rhodobacter sphaeroides*. *Biochemistry.* 36:2300–2306.

Ogawa, K., T. Zhang, K. Yoshihara, and Y. Kobuke. 2002. Large third-order optical nonlinearity of self-assembled supramolecular porphyrin oligomers. *J. Am. Chem. Soc.* 124:22–23.

Orädd, G., G. Lindblom, G. Arvidson, and K. Gunnarsson. 1995. Phase equilibria and molecular pacing in the *n,n*-dimethyldodecylamine oxide/gramicidin D/water system studied by ²H nuclear magnetic resonance spectroscopy. *Biophys. J.* 68:547–557.

Prince, S. M., T. D. Howard, D. A. A. Myles, C. Wilkinson, M. Z. Papiz, A. A. Freer, R. J. Cogdell, and N. W. Isaacs. 2003. Detergent structure in crystals of the integral membrane light-harvesting complex LH2 from *Rhodopseudomonas acidophila* strain 10050. *J. Mol. Biol.* 326:307–315.

Polivka, T., T. Pullerits, J. L. Herek, and V. Sundström. 2000. Exciton relaxation and polaron formation in LH2 at low temperature. *J. Phys. Chem. B.* 104:1088–1096.

Pullerits, T., M. Chachisvilis, and V. Sundström. 1996. Exciton de-localization length in the B850 antenna of *Rhodobacter sphaeroides*. *J. Phys. Chem. B.* 100:10787–10792.

Reddy, N. R. S., R. Picorel, and G. J. Small. 1992. B896 and B870 components of the *Rhodobacter sphaeroides* antenna: a hole-burning study. *J. Phys. Chem.* 96:6458–6464.

Rogl, H., K. Kosemund, W. Kühlbrandt, and I. Collinson. 1998. Refolding of *Escherichia coli* produced membrane protein inclusion bodies immobilised on nickel chelating chromatography. *FEBS Lett.* 432:21–26.

Roth, M., A. Lewit-Bentley, H. Michel, J. Deisenhofer, R. Huber, and D. Oesterhelt. 1989. Detergent structure in crystals of a photosynthetic reaction centre. *Nature.* 340:659–661.

Scholes, G. 1999. Theory of coupling in multichromophoric systems. *In* Resonance Energy Transfer. D. L. Andrews and A. A. Demidov, editors. John Wiley and Sons, New York, NY. 213–242.

Sirringhaus, H., P. J. Brown, R. H. Friend, M. M. Nielsen, K. Bechgaard, B. M. W. Langeveld-Voss, A. J. H. Spiering, R. A. J. Janssen, E. W. Meijer, P. Herwig, and D. M. de Leeuw. 1999. Two-dimensional charge transport in self-organized, high-mobility conjugated polymers. *Nature.* 401:685–688.

Sundström, V., T. Pullerits, and R. van Grondelle. 1999. Photosynthetic light-harvesting: reconciling dynamics and structure of purple bacterial LH2 reveals function of photosynthetic unit. *J. Phys. Chem. B.* 103:2327–2346.

Tanford, C. 1997. How protein chemists learned about the hydrophobic factor. *Protein Sci.* 6:1358–1366.

Trinkunas, G., J. L. Herek, T. Polivka, V. Sundström, and T. Pullerits. 2001. Exciton delocalization probed by excitation annihilation in the light-harvesting antenna LH2. *Phys. Rev. Lett.* 86:4167–4170.

Unwin, P. N., and R. Henderson. 1975. Molecular-structure determination by electron-microscopy of unstained crystalline specimens. *J. Mol. Biol.* 94:425–440.

van Grondelle, R., C. N. Hunter, J. G. C. Bakker, and H. J. M. Kramer. 1983. Size and structure of antenna complexes of photosynthetic bacteria as studied by singlet-singlet quenching of the bacteriochlorophyll fluorescence yield. *Biochim. Biophys. Acta.* 723:30–36.

Valkunas, L., G. Trinkunas, V. Liuolia, and R. van Grondelle. 1995. Nonlinear annihilation of excitations in photosynthetic systems. *Biophys. J.* 69:1117–1129.

Vasilescu, M., P. Angelescu, M. Almgren, and A. Valstar. 1999. Interactions of globular proteins with surfactants studied with fluorescence probe methods. *Langmuir.* 15:2635–2643.

Vos, M., R. van Grondelle, F. W. van der Kooij, D. van de Poll, J. Amesz, and L. N. M. Duysens. 1986. Singlet-singlet annihilation at low temperatures in the antenna of purple bacteria. *Biochim. Biophys. Acta.* 850:501–512.

Westerhuis, W. H. J., M. Vos, R. van Grondelle, J. Amesz, and R. A. Niederman. 1998. Altered organization of light-harvesting complexes in phospholipid-enriched *Rhodobacter sphaeroides* chromatophores as

determined by fluorescence yield and singlet-singlet annihilation measurements. *Biochim. Biophys. Acta.* 1366:317–329.

Wolf-Klein, H., C. Kohl, K. Müllen, and H. Paulsen. 2002. Biomimetic model of a plant photosystem consisting of a recombinant light-harvesting complex and a terrylene dye. *Angew. Chem. Int. Ed.* 41:3378–3380.

Young, A. J. 1991. The photoprotective role of carotenoids in higher plants. *Physiol. Plant.* 83:702–708.